Order and strain in main-chain smectic liquid-crystalline polymers and elastomers

W.H. de Jeu[1,a], E.P. Obraztsov[1], B.I. Ostrovskii[1,2], W. Ren[3], P.J. McMullan[3], A.C. Griffin[3], A. Sánchez-Ferrer[4], and H. Finkelmann[4]

[1] FOM Institute for Atomic and Molecular Physics, Kruislaan 407, 1098 SJ Amsterdam, The Netherlands
[2] Institute of Crystallography, Academy of Sciences of Russia, Leninsky prospect 59, 117333 Moscow, Russia
[3] School of Polymer, Textile and Fiber Engineering, Georgia Institute of Technology, Atlanta, GA 30332, USA
[4] Institut für Makromolekulare Chemie, Universität Freiburg, D-79104 Freiburg, Germany

Abstract. The layer correlations in main-chain smectic liquid-crystal polymer and elastomer systems have been studied using high-resolution X-ray scattering. In contrast to side-chain smectic polymers, in main-chain systems the polymer chains are oriented parallel to the layer normal. As a result they couple directly to the lamellar structure and any polymer defect is translated into layer distortions. For the homopolymers the resulting X-ray lineshapes are well described by Lorentzians. This is interpreted as an average of algebraically decaying order in domains with dimensions of hundreds of nm and a wide dispersion of sizes. The elastomers show much broader peaks than the correponding polymers. This is attributed to strong non-uniform strain within the finite-size domains due to defects of the layer structure.

PACS. 64.60.Cn Order-disorder transformations; statistical mechanics of model systems – 61.10.Eq X-ray scattering (including small-angle scattering) – 61.41.+e Polymers, elastomers, and plastics – 61.30.Eb Experimental determinations of smectic, nematic, cholesteric, and other structures

1 Introduction

Long-range translational order can be strongly disrupted when a system is exposed to an external random field [1]. At large enough length scales imposing even weak disorder can destroy the translational symmetry. Classical examples stem from the pinning of flux vortex lattices in a superconductor by impurities [2] and from magnetism (disordered Ising magnets) [3]. Here we are concerned with more recent applications to liquid-crystal (LC) physics, in particular to smectic systems that consist of regular stacks of fluid monolayers. Clark and coworkers [4] have shown that when monomeric smectic systems are confined to aerogels, the random field imposed by the confinement reduces the smectic layer correlations to short range. Smectic monomers [5] and polymers [6] provide interesting model examples for various types of transitions because of the low-dimensional character of their ordering. The associated fluctuations cause the mean-squared displacements of the layer positions to diverge logarithmically with the system size [1,7,8] (Landau-Peierls instability). As a result the positional correlation function

[a] *Present address*: Polymer Science and Engineering, University of Massachusetts, 120 Governors Drive, Amherst, MA 01003, USA; e-mail: dejeu@mail.pse.umass.edu
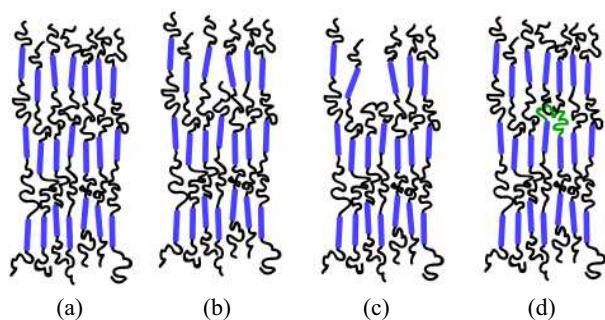
describing the smectic layer periodicity decays at large distances as $r^{-\eta}$, the exponent η being small and positive (quasi-long-range order). Smectic polymers can be crosslinked to form smectic elastomers [9]. In earlier work we showed that the internal random field of distortions due to this process can again lead to disorder, but only at relatively large crosslink density [10,11].

The quasi-long-range order of conventional smectic systems can be studied by high-resolution X-ray scattering. Instead of delta-function–type Bragg peaks with diffuse tails characteristic of a three-dimensional (3D) crystal periodicity, Caillé lineshapes with an asymptotic power law form $q^{-2+n^2\eta}$ are observed [1,12,13]. Here n represents the harmonic number of the quasi-Bragg peak. The scaling of the exponent η with n^2 is an important experimental signature of quasi-long-range order. As these arguments are essentially related to the layer symmetry, they apply equally well to smectic-A systems (Sm-A, density wave parallel to the layer normal) as to smectic-C systems (Sm-C, density wave tilted with respect to the layer normal). This general behaviour of low-molecular-mass smectics is essentially conserved in smectic polymers [14]. When in turn LC polymers are weakly crosslinked into an elastomer network, the macroscopic rubber elasticity [9] interacts with the smectic LC order. This gives

Fig. 1. Cartoons of a main-chain smectic polymer. (a) Text-book picture; (b) end defect; (c) hairpin; (d) entangled hairpin.

rise to a rich behaviour that has been well studied for smectic side-chain elastomers. First, crosslinks suppress long-wavelength fluctuations leading to the possibility of true long-range order [15,16]. Second, crosslinks preferentially reduce the smectic density around their position, giving rise to a random field of defects that can destroy the smectic order [10,17,18]. In contrast to smectic side-chain elastomers very little is known about the order in smectic main-chain systems.

In side-chain smectic LC polymers and elastomers the polymer backbone is approximately confined (or at least concentrated) in 2D to the space in between the smectic layers. In that situation the overall polymer structure can be either prolate or oblate (see Ref. [19] for a review). Nevertheless due to the freedom in 2D, polymer conformations and defects are not expected to interact directly with the smectic layer order. This can be contrasted with main-chain smectic polymers (Fig. 1a) that consist of alternating flexible polymer parts and rigid smectogenic elements. Now the polymer chain is not only on average oriented parallel to the smectic layer normal but also connecting the smectic layers. As a result, polymer defects are expected to be directly translated into layer distortions (Fig. 1b–d).

In this paper we discuss the nature of the ordering in smectic main-chain systems, both polymers and elastomers, elaborating on and correcting an earlier communication [20]. The layer diffraction from the homopolymers can be —somewhat unexpectedly— described by a Lorentzian lineshape that is interpreted as an average of algebraically decaying order in domains of the order of hundreds of nm and with a wide dispersion of sizes. The elastomers show much broader peaks; this is attributed to strong nonuniform strain due to lattice defects reducing the apparent dimensions of the finite-size domains to tens of nm.
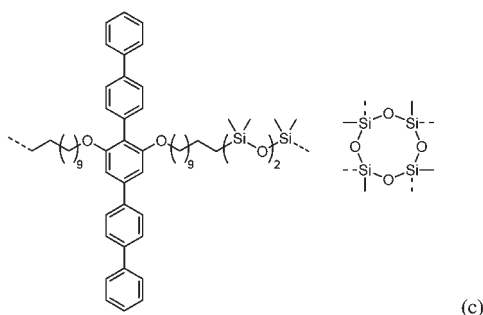
2 Experimental

The main-chain smectic polymer and elastomer systems used in this study are depicted in Figure 2 together with their phase behaviour. The first system [21] (denoted as MC11; from Freiburg) has $M_n \simeq 14000$, $M_w/M_n \simeq 2.8$ and an average degree of polymerization $DP \simeq 20$ with
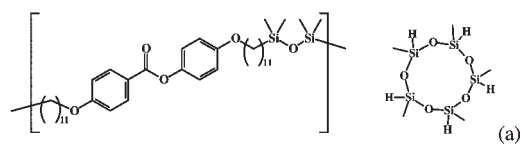
MC11-pol: K 50°C Sm-C 95°C I
MC11-el: K 41°C Sm-C 110°C I
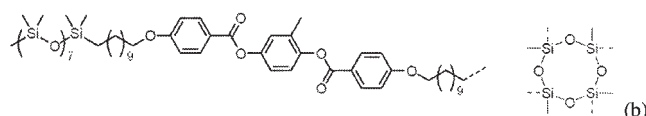
MeHQ-pol: g −33°C Sm-C 98°C I
MeHQ-el: g −25°C Sm-C 104°C I

TR5-el: Sm-C 52°C I
No glass transition was detected

Fig. 2. Molecular structure of the main-chain smectic polymer MC11 (a), MeHQ (b) and TR5 (c). The polymer structure as given at the left is converted to the elastomer by adding about 10% of the crosslinker at the right.

for MC11-el about 10% crosslinks. Note the mutifunctional character of the crosslink unit that can connect up to five polymer chains. At temperatures above 40–50 °C a tilted Sm-C phase is observed. Oriented elastomer samples (typically $20 \times 10\,\mathrm{mm}^2$ and $0.5\,\mathrm{mm}$ thick) were obtained through uniaxial deformation during the completion of the network. The Sm-C layers were arranged conically under a tilt angle with respect to the direction of the applied stress (texture axis: long direction of the sample). The second example (denoted as MeHQ; from Atlanta) has $M_n \simeq 24600$, $M_w/M_n \simeq 2.1$ and an average degree of polymerization $DP \simeq 17$ with for MeHQ-el about 10% crosslinks. It is chemically rather similar to MC11 but has the Sm-C phase at room temperature. However, note that the rigid mesogenic groups now are connected by an alkyl chain to a short siloxane polymer. Hence compared to MC11 the mesogenic groups in MeHQ are much more weakly coupled. In this case the elastomer sample was strained up to 200%. The uniform orientation thus obtained is maintained at room temperature: plastic deformation starts at about 45%. The original length can recover in aid of heat or appropriate solvent. The third and final system (denoted as TR5; from Atlanta) has a Sm-A phase below about 50 °C. For this material the long

direction of the sample coincides with the layer normal. This material is rather peculiar because of the presence of transverse pentaphenyl rods [22]. To maintain the Sm-A symmetry the rods are expected to orient locally parallel to the smectic layer normal, similarly in laterally substituted low-molecular mass systems [23]. As was found for MeHQ-el, the TR5-el maintains a uniform orientation at room temperature after stretching. In conclusion all three elastomer samples could be investigated in a uniformly aligned smectic state in a transmission X-ray geometry; MC11 at 60 °C, MeHQ and TR5 at room temperature.

Homopolymer films were prepared at temperatures close to the smectic-isotropic transition by moving a spreader over a drop of material on a glass substrate to give films with a thickness of about 100 μm. Though the uniformity was rather variable, X-ray data could easily be taken in a reflectivity configuration.

The samples were preliminary characterized using an in-house setup with a rotating anode X-ray generator (Rigaku RU-300H, 18 kW) equipped with two parabolic multi-layer mirrors (Bruker, Karlsruhe), giving a highly parallel beam of monochromatic CuK_α radiation (λ = 0.154 nm) with a divergence of about 0.02 °. The smectic layer structure could easily be determined using a 2D detector (Bruker Hi-star) at a distance of about 0.6 m from the sample stage. More importantly, the in-plane order in the WAXS region was recorded by a linear position-sensitive detector (PSD-50M, M. Braun, Germany), which could be rotated around the beam path to measure in either the meridianal or the equatorial direction.

High-quality X-ray lineshapes of the layer correlations were taken at the Exxon beamline X10A at the National Synchrotron Light Source, Brookhaven National Laboratory (Upton, NY, USA) and at beamline W1 of Hasylab (DESY, Hamburg, Germany). In both cases 8 keV radiation was used corresponding to a wavelength λ = 0.155 nm. The wave vector transfer is given by $\mathbf{q} = \mathbf{k}_f - \mathbf{k}_i$, where $\mathbf{k}_f$ and $\mathbf{k}_i$ are the outgoing and incoming wave vector, respectively, with $q = |\mathbf{q}| = (4\pi/\lambda)\sin\theta$, 2θ being the scattering angle. The scattering plane ((z, x)-plane) was vertical with the q_z-axis initially parallel to the smectic layer normal. Hence for a Sm-A phase quasi-Bragg peaks of harmonic number n were measured in the reciprocal space along q_z at positions q_n, while the mosaic distribution was determined by transverse (rocking) curves varying q_x at different $q_z = q_n$. In case of a Sm-C phase the sample was rotated over the tilt angle with respect to the texture axis. This brings one of the Sm-C layer reflections from the cone distribution along q_z, leading to a situation similar as for Sm-A.

The instrumental resolution in the scattering plane was set by a double-bounce Ge(111) (at the NSLS) or Si(111) monochromator (at Hasylab) and a double- or triple-reflection channel-cut Ge(220) or Si(111) analyzer crystal in a non-dispersive configuration. The resulting resolution function was close to a Gaussian with Δq_z = 0.004 nm^{-1} (full-width-at-half-maximum, FWHM). The resolution function along q_x could be taken as a δ-function. Out of the scattering plane the resolution

(a)

(b)

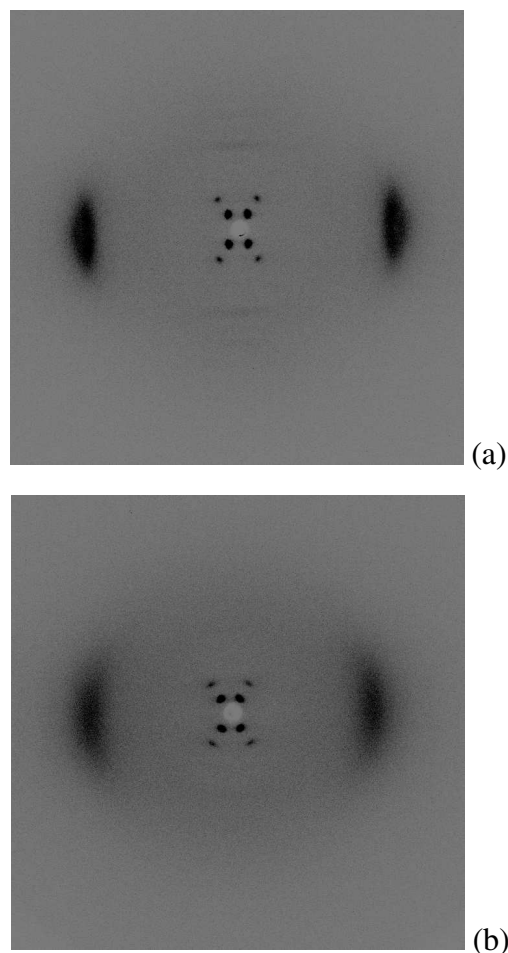**Fig. 3.** X-ray picture of the elastomer MC11-el at 23 °C (a) and 70 °C (b).

was set by slits to Δq_y = 0.02 nm^{-1}. The incident intensity was about 5×10^9 cts/s; the beam size was 0.5×1 mm^2 (V×H). All data were normalized, resolution corrected and background subtracted. The latter point is a crucial aspect for the present precise lineshape measurements including the tails of the peaks. It requires to distinguish the $\mathbf{q}$-dependent spatial background in the hutch from the time-dependent dark current of the scintillation counter. This was done by calculating the normalized q-dependent background by substracting the time dependent part. After correcting the data for this "bare" background, subsequently the time-dependent part was subtracted taking the actual measurement time into account.

3 Results

3.1 Characterisation of the smectic phases

Figure 3 gives a photographic X-ray overview of the MC11-el system that clearly shows the splitting off-axis of the smectic peak typical for a Sm-C phase. The in-plane scattering of Figure 4 indicates for both the homopolymer and the elastomer crystalline ordering below the phase
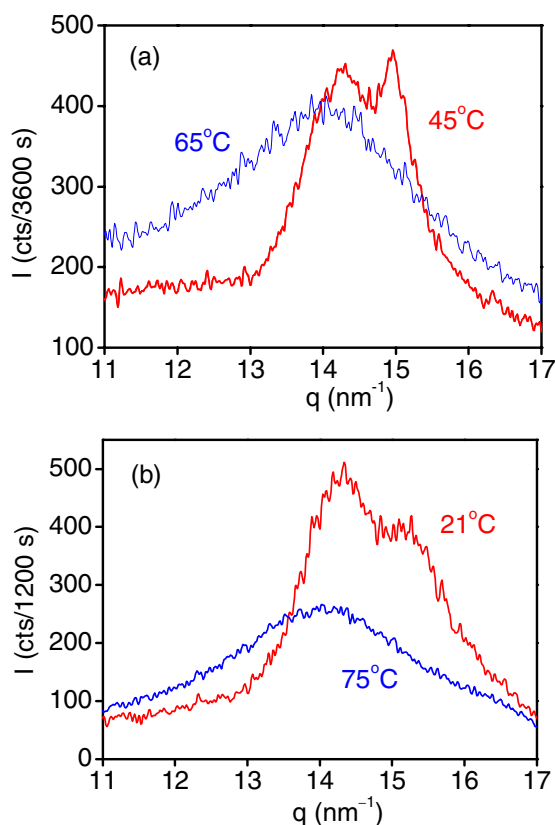
Fig. 4. In-plane order of the smectic layers of the homopolymer MC11-pol (a) and the elastomer MC11-el (b).
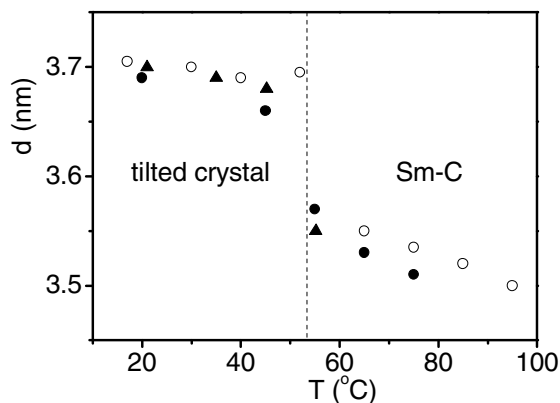

Fig. 5. Smectic layer period for two different samples of the homopolymer MC11-pol (open and filled symbols). The vertical line indicates the phase transition temperature. Circles: heating; triangles: cooling.

transition around $50\,^{\circ}$C. The splitting into two peaks, corresponding to periodicities of 0.42 and 0.44 nm, respectively, points to a tilted crystalline phase with a rectangular in-plane lattice. For the homopolymer the finite-size broadened crystalline peaks can be fitted by Gaussians leading to a domain size of $\sim 15\,$nm. Above the transition liquid peaks are observed that can be fitted by a Lorentzian centered at $q = 14\,\mathrm{nm}^{-1}$ ($2\pi/q = 0.45\,$nm) and
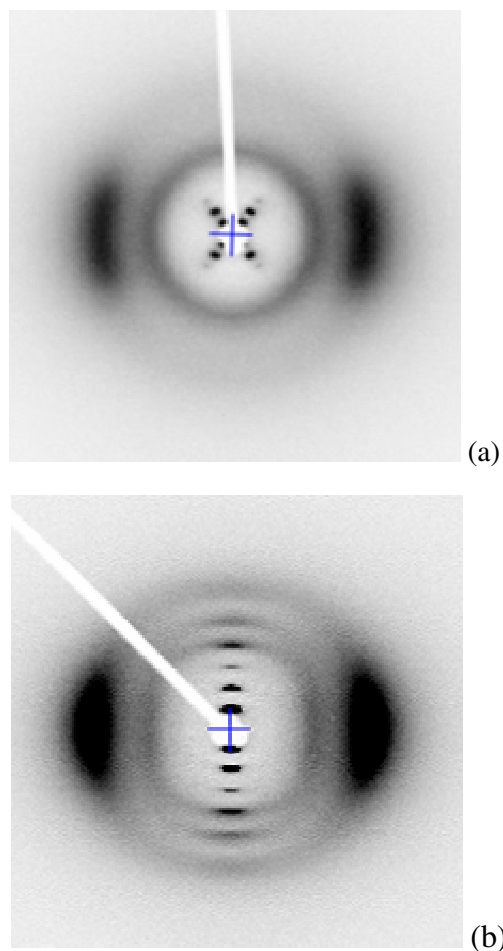
Fig. 6. X-ray picture of the elastomers MeHQ-el (a, Sm-C) and TR5-el with pentaphenyl transverse rods (b, Sm-A) stretched at room temperature.

a correlation length of $\sim 1\,$nm. The in-plane melting leads to a decrease of the smectic layer period as shown in Figure 5. Because of these results, we have chosen a temperature of $60\,^{\circ}$C for the investigation of the Sm-C lineshape.

In Figure 6a we show an X-ray overview of the MeHQ-el system at room temperature. The general behaviour is very much the same as observed for MC11-el at higher temperatures: Sm-C with liquid in-plane ordering. However, in addition to the strong equatorial liquid peak an additional ring is visible at smaller angles with some increased intensity along the equator. The corresponding period of 0.7 nm is typical for siloxanes and indicates some form of lamellar micro-phase separation of the central siloxane parts. The corresponding homopolymer MeHQ-pol displays a sharp smectic peak and a broad in-plane one (not displayed), indicating stacked liquid layers at a period of 4.5 nm. Finally we give in Figure 6b an overview of the TR5-el system. Along the meridian we note a large number of harmonics indicating strong Sm-A order with again a liquid in-plane structure. At large q-values the situation is more complicated, which is related to the packing of the transverse rods. This is an interesting problem by itself, but outside the scope of this work for which only the

Sm-A symmetry of the phase is of importance. The polymer TR5-pol showed below the transition to the isotropic phase at 52 °C stacked crystalline layers with either a single or a double periodicity (3.15 and 6.3 nm, respectively). The latter structures depended on the history of the sample and have not been further investigated.

3.2 Lineshape analysis

The total intensity measured in X-ray scattering of smectic systems can be written as the following convolution of various factors [24]:

$$I(q) = S(\mathbf{q}) \otimes H(\mathbf{q}) \otimes F(q_\perp) \otimes R(\mathbf{q}). \tag{1}$$

In this equation $S(\mathbf{q})$ is the smectic structure factor, $H(\mathbf{q})$ stands for broadening due to finite sizes, $F(q_\perp)$ represents the effect of the mosaic distribution that can me measured in-plane along $q_\perp$ while finally $R(\mathbf{q})$ results from the resolution of the diffractometer. In principle all these contributions can be incorporated in an effective experimental resolution function $R'(\mathbf{q}) = F \otimes H \otimes R$ with a different full-widt-at-half-maximum (FWHM) in all three dimensions. Deconvolution of the experimental data with $R'(\mathbf{q})$ then provides the required determination of $S(\mathbf{q})$.

Size effects come in because the stacking of smectic layers in real samples is limited: the maximal domain size observed in low-molecular-mass thermotropic smectics is of the order of some tens of μm. From our previous experience with side-chain siloxane elastomers [10,11] we know that the distribution and magnitude of the domains along the layer normal, $H(z)$, are of prime importance for the lineshape analysis. Depending on the polymer topology and/or crosslink density the domain size distribution function can be either narrow or rather broad. To describe this variable situation empirically, we have introduced a stretched Gaussian correlation function of the form

$$G(z) \propto \exp\left[\frac{-\left(\sigma^2 z^2\right)^\beta}{2\beta}\right], \tag{2}$$

in which the parameter β determines the degree of stretching. Such a stretched Gaussian (or compressed exponential) interpolates between a Gaussian for $\beta = 1$ and an exponential correlation for $\beta = 0.5$. While the Fourier transform of a Gaussian is still a Gaussian, exponential correlation leads in 1D to a Lorentzian structure factor:

$$I(q) \propto \left[\left(q - q_0\right)^2 + k^2\right]^{-1}, \tag{3}$$

with a correlation length $\xi = k^{-1}$. Figure 7 illustrates the relatively narrow distribution and the very broad one corresponding to these limiting cases. Intermediate values of β evidently lead to less pronounced wings than found for a pure Lorentzian. Figure 8 shows that over the whole range of q-values the lineshape is strongly influenced by the contribution of the stretched Gaussian. Figure 8a demonstrates the effect of the degree of stretching (decreasing value of β) on the tails of the peaks; Figure 8b indicates how the various harmonics are affected.
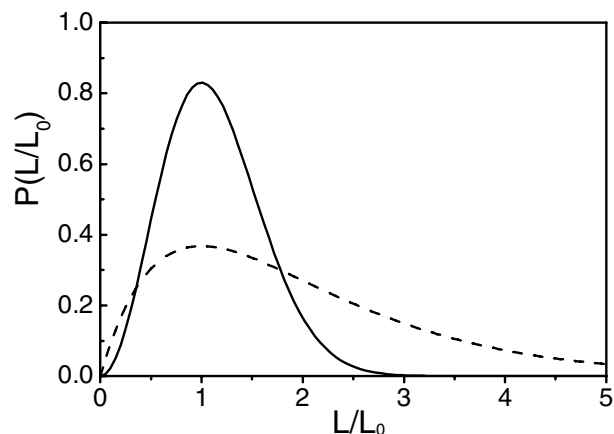

Fig. 7. Model domain sizes distributions. Broken line corresponds to a distribution resulting in exponential decay ($\beta = 0.5$), solid line to a distribution resulting in a Gaussian ($\beta = 1.0$).
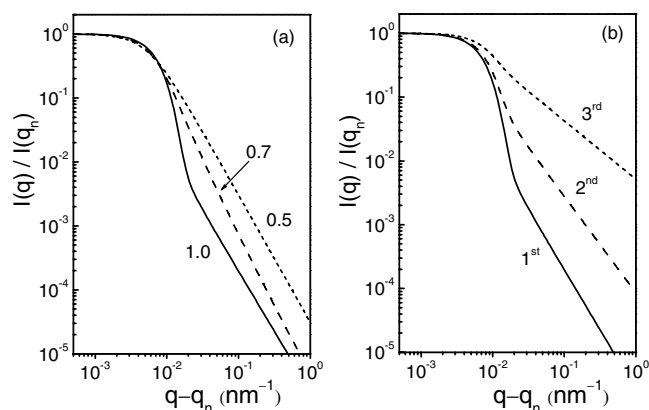

Fig. 8. Model profiles showing the disappearance of the fracture in the lineshape for $\eta = 0.12$ and a fixed finite size $\Delta q_z = 0.01\,\mathrm{nm}^{-1}$ ($L = 0.6\,\mu$m). (a) First-order lineshape for a stretched Gaussian with different β-values as indicated. (b) Variation of lineshape with harmonic number.

The finite-size determined center of the X-ray peaks continues at larger values of $q_z - q_n$ into a slope controlled by the mosaic distribution. If this distribution is small one can clearly identify the limiting Caillé slope determined by the exponent $2 - n^2\eta$. Alternatively for a "powder" distribution of orientations $1 - n^2\eta$ applies. In the present case we have rather uniformly oriented samples but still with relatively large mosaic distributions, which makes it somewhat questionable whether the first limit can be reached. The problems involved in a complete description in terms of equation (1) have been discussed in some detail elsewhere [11]. Here we shall restrict ourselves to an empirical approach and concentrate on the finite size effect and the Caillé limit.

With these considerations in mind we present in the next series of figures in some detail the X-ray lineshapes of the various harmonics of the different samples. We shall systematically give combinations of two figures: first a conventional X-ray peak (intensity I *vs.* q_z) is shown, normalized to the maximum intensity on a logarithmic
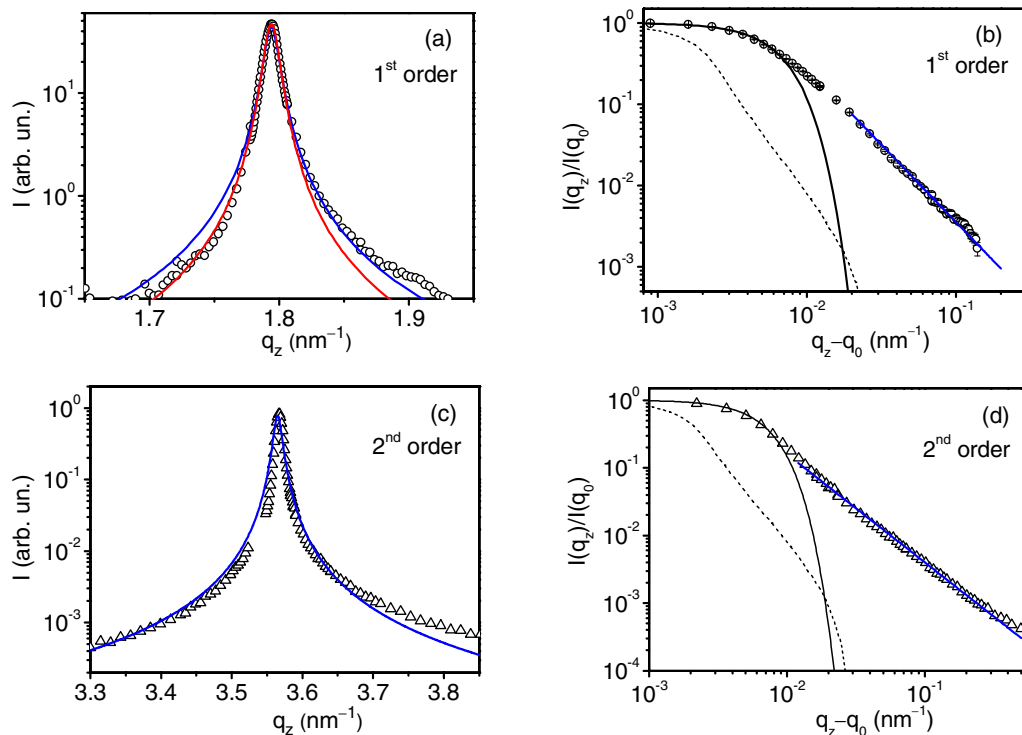
Fig. 9. First-order (a, b) and second-order (c, d) peak of the homopolymer MC11-pol in the Sm-C phase at 60 °C. Left panels: Lorentzian fit in blue, stretched Gaussian correlation ($\beta = 0.54$) in red. Right panels: Gaussian in black, large-q Caillé limit in blue, broken line indicates the direct beam.
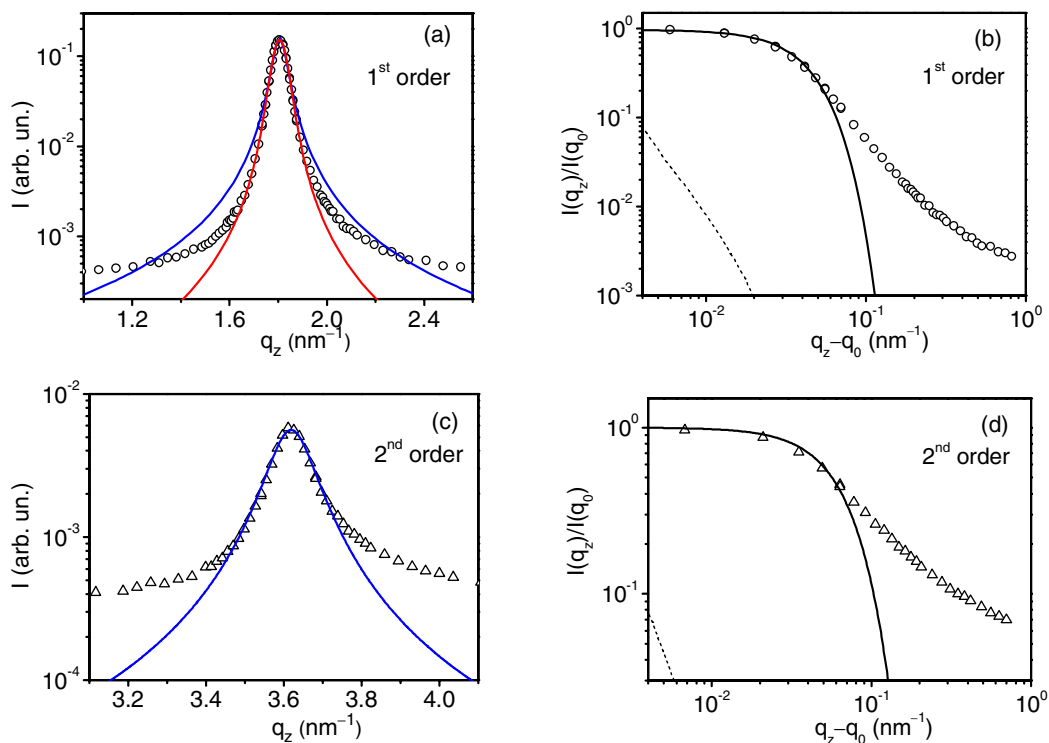

Fig. 10. First-order (a, b) and second-order (c, d) peak of the elastomer MC11-el in the Sm-C phase at 60 °C. Left panels: Lorentzian fit in blue, stretched Gaussian correlation ($\beta = 0.71$) in red. Right panels: Gaussian in black, broken line indicates the direct beam. No consistent Caillé limit can be given.
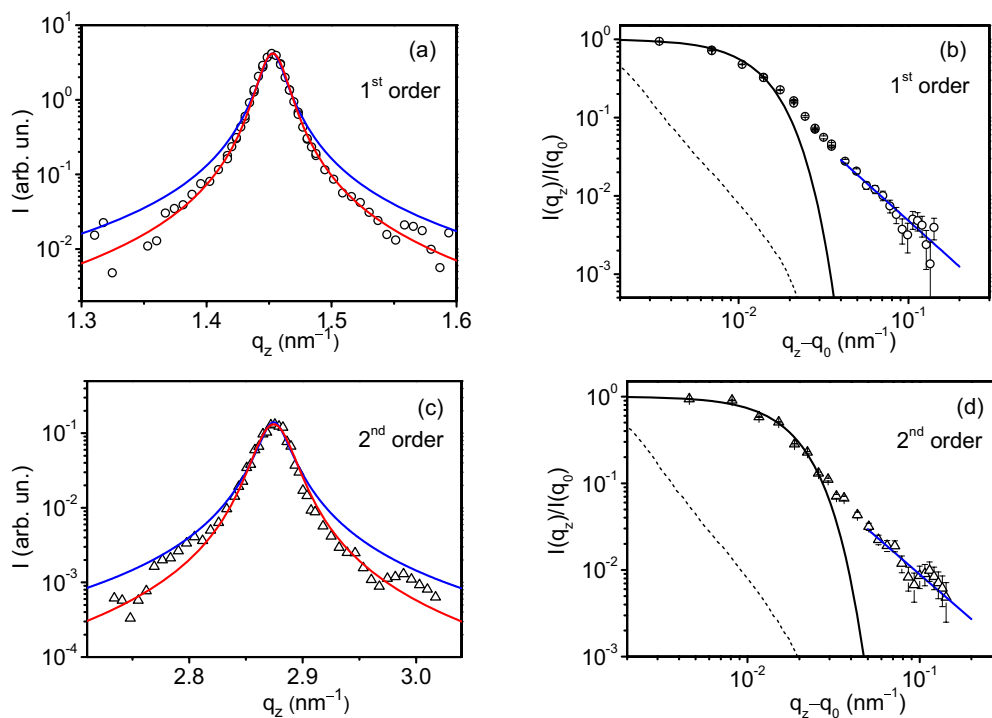
Fig. 11. First-order (a, b) and second-order (c, d) peak of the homopolymer MeHQ-pol in the Sm-C phase. Left panels: Lorentzian fit in blue, stretched Gaussian correlation ($\beta = 0.61$ and 0.65, respectively) in red. Right panels: Gaussian in black, large-q Caillé limit in blue, broken line indicates the direct beam.
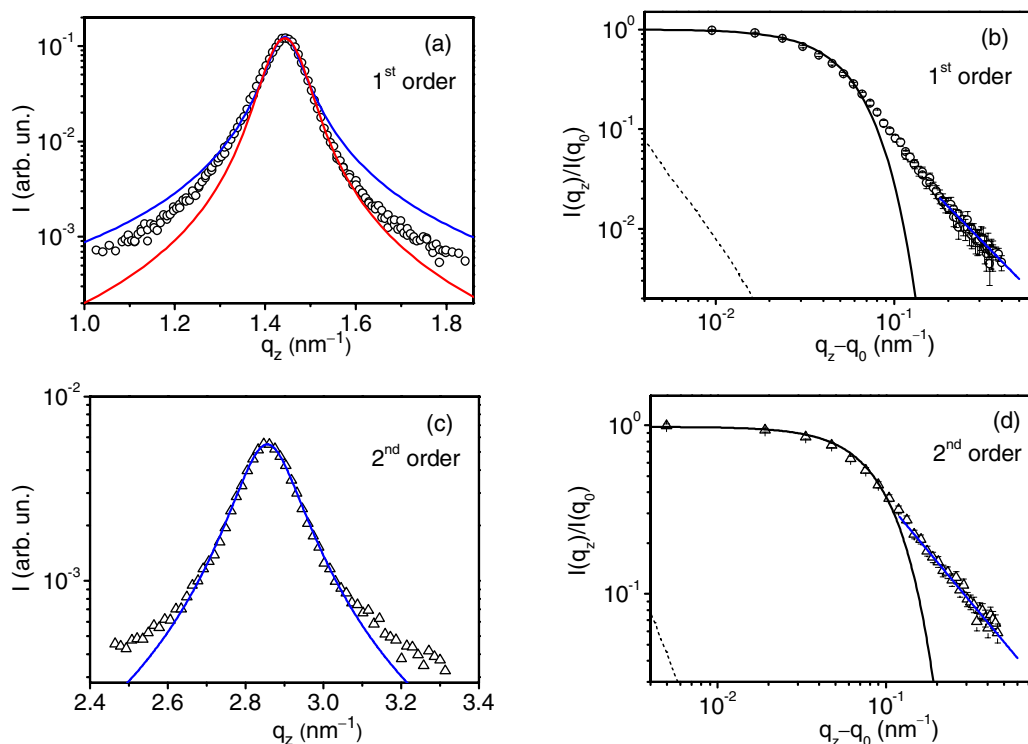

Fig. 12. First-order (a, b) and second-order (c, d) peak of the elastomer MeHQ-el in the Sm-C phase. Left panels: Lorentzian fit in blue, stretched Gaussian correlation ($\beta = 0.71$) in red. Right panels: Gaussian in black, large-q Caillé limit in blue, broken line indicates the direct beam.
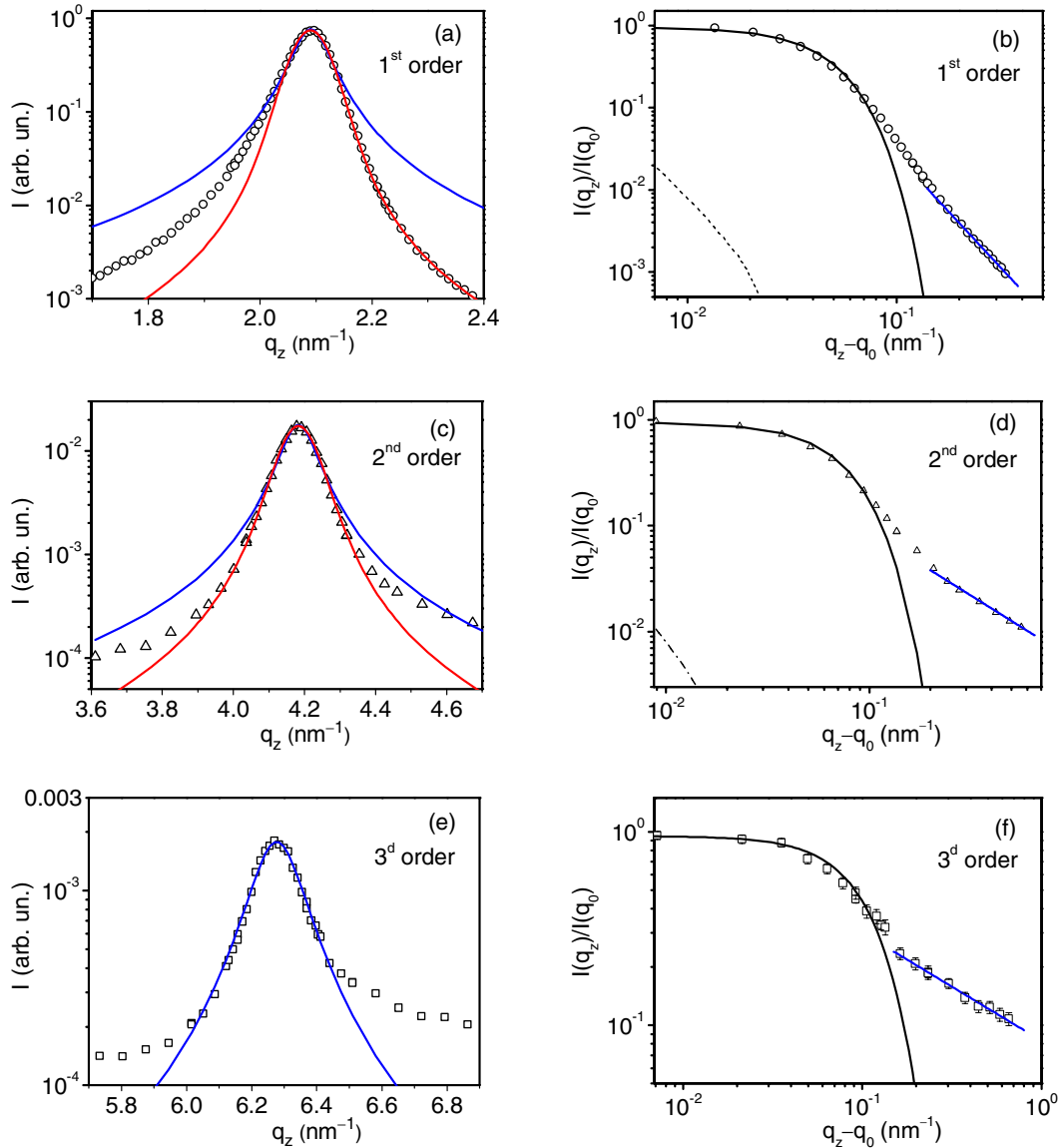
Fig. 13. Lineshape for three harmonics of the elastomer TR5-el in the Sm-A phase. Left panels: Lorentzian fit in blue, stretched Gaussian correlation ($\beta = 0.82$ and 0.71, respectively) in red. Right panels: Gaussian in black, large-q Caillé limit in blue, broken line indicates the direct beam.

scale. In addition a double-logarithmic figure is given emphasizing the behaviour of the tails. Figures 9 and 10 show the lineshape results for two harmonics from the Sm-C lamellar order at about 62 °C of MC11-pol and MC11-el, respectively. We want to emphasize that these results differ from earlier ones presented by us [20]. In fact these earlier results refer to the room temperature tilted crystalline phase and not to the Sm-C phase. This unfortunate error stems from a miscommunication regarding the temperature of the measurements. For the homopolymer MeHQ-pol and for the corresponding elastomer two harmonics could be measured (Figs. 11 and 12). Finally Figure 13 shows three harmonics for the Sm-A peak of the elastomer TR5-el.

All the right (double-logarithmic) figures show an attempt to fit a straight line at large q-values, allowing to test the Caillé limit predicting a decay according to $(q - q_n)^{-2+n^2\eta}$. In addition the central part of the X-ray peak has been fitted to a Gaussian function constraint to reproduce the experimental FWHM Δq_z. This value can be interpreted as an average finite domain size according to $L = 2\pi/\Delta q_z$. Furthermore empirical attempts were made to fit each full curve by a Lorentzian and by a stretched Gaussian. The results of these exercises are summarized in Table 1 in which also the smectic periodicity $d = 2\pi/q_0$ and the mosaic distribution of each of sample is given. Note that for the elastomers (not for the polymers) Δq_z scales approximately linearly with the harmonic number n.

Table 1. Summary of fitting results for the elastomers and some corresponding homopolymers. The domain size is calculated as $L = 2\pi/\Delta q_z$.

Sample	Harmonic order n	$d \pm 0.02$ (nm)	FWHM Δq_z ($10^{-3}\,\text{nm}^{-1}$)	Domain size L (nm)	Mosaic spread (deg)
MC11-pol	1	3.50	11	550	8
MC11-pol	2	3.52	12	540	
MeHQ-pol	1	4.33	22	290	9.5
MeHQ-pol	2	4.37	30	210	
MC11-el	1	3.48	71	88	10
MC11-el	2	3.47	122	52	
MeHQ-el	1	4.35	88	71	11
MeHQ-el	2	4.40	171	37	
TR5-el	1	3.01	80	79	13
TR5-el	2	3.00	130	48	
TR5-el	3	3.00	189	33	

4 Discussion

The FWHM Δq_z of the quasi-Bragg peaks is in none of the samples resolution limited and the central part can usually be well described by a Gaussian. This leads to finite sizes along the layer normal of the order of hundreds of nm for the polymers and tens of nm for the elastomers (see Tab. 1). For the homopolymers Δq_z is constant for both harmonics of MC11-pol and increases slightly for MeHQ-pol. Possibly in the latter case some internal strain developed during the cooling to room temperature which is absent for MC11-pol in the smectic phase at temperatures around $60\,^{\circ}\text{C}$.

Next we consider fitting the wings of the polymer peaks in a double-logarithmic plot to straight lines. For MC11-pol we can fit both harmonics to an exponent $2 - n^2\eta$ with $\eta = 0.10$ (Fig. 9, right). For MeHQ-pol the situation is slightly more complicated. The first and the second harmonic lead to $\eta = 0.05$ and $\eta_2 = 0.28$, respectively (Fig. 11, right). This is in principle compatible with scaling according to $2 - n^2\eta$ with $\eta = 0.06 \pm 0.01$. Hence in the main-chain smectic polymers algebraic decay appears to be maintained within the smectic domains.

Somewhat unusually for smectic systems [4,10,11] for MC11-pol and MeHQ-pol the overall lineshape can be reasonably well fitted by a Lorentzian, equation (3), with a correlation length ξ that is of the same order for both harmonics. The arising interpretation of a Lorentzian as indicating short-range order can be excluded for two reasons. First the correlation lengths are large, of the order of hundreds of nm. More importantly, for short-range order hardly higher harmonics are expected as the width Δq of the successive harmonics increases as n^2. This leaves as the most plausible explanation that the Lorentzian lineshape is due to a broad exponential-like distribution of domain sizes in the sample, see Figure 7. Such situations have been well documented in powder diffraction (see, for example Ref. [25]). The specific nature of the distribution

(as compared to other smectic systems) could arise from the direct coupling between polymer defects and smectic layer correlations that is typical for smectic main-chain systems only. A first candidate for such defects are hairpins (Fig. 1c) [26–28]. However, stress-strain experiments on nematic main-chain networks indicate that during the formation of a monodomain sample simple hairpins are probably removed by the mechanical strain and might play only a minor role [29]. On the other hand, this argument does not hold anymore for entangled hairpins as depicted in Figure 1d. The presence of such defects would be compatible with a plateau in the stress-strain curve. Additionally chain ends may play a role. Analogous to the situation described for the nematic phase [30], these could also lead to local distortion of the smectic layers (Fig. 1b). Contrary to side-chain smectic polymers, the polymer chains in main-chain systems contribute to the building of the smectic layers themselves. Due to dispersion of the polymer chain length the layered structure in the direction along layer normals cannot be terminated at any arbitrary place thus leading to a finite-size dispersion. Inside the domains/grains leading to the Lorentzian average still algebraic decaying smectic order appears to be present.

Next we come to the three elastomer samples: MC11-el (Sm-C, Fig. 10), MeHQ-el (Sm-C, Fig. 12) and TR5-el (Sm-A, Fig. 13). In these cases the domain sizes as measured (tens of nm) are appreciably smaller than for the corresponding polymers. The broadening of the smectic peaks with increasing harmonic number n is very similar as observed in smectic side-chain elastomer systems [10,11]. In the latter situation the broadening has been attributed to strain due to the layer displacements around the crosslinks or other types of defects generated by the crosslinks. The linear increase in Δq_z for the elastomers points to strain-induced broadening of the X-ray peak [31–33], We recall that two effects may contribute to broadening of the X-ray peak: the finite size of crystalline or smectic domains (grains) in the sample and a

possible non-uniform strain within each domain induced by lattice defects. The strain broadening of a diffraction peak is proportional to the length of the scattering vector, while the size effect does not depend on it. Thus comparing the peak widths of successive harmonics both contributions can be separated. These effects have been well documented in metal physics, in particular for metals subjected to cold work (see for a critical discussion Ref. [34]). The total contribution to the Gaussian linewidth can be written as

$$\Delta q_{\exp}^2 = \Delta q_{\mathrm{intrinsic}}^2 + n^2 \Delta q_\varepsilon^2 + \Delta q_{\mathrm{beam}}^2. \qquad (4)$$

In this formula ε refers to the strain and the contribution $\Delta q_{\mathrm{beam}} \simeq 4 \times 10^{-3}\,\mathrm{nm}^{-1}$ from the direct beam can usually be neglected. Applying this formula to the results of Table 1 we find for $\Delta q_{\mathrm{intrinsic}}$ the values given in Table 2. The corresponding numbers of $L_{\mathrm{intrinsic}} = 2\pi/\Delta q_{\mathrm{intrinsic}}$ are of the same order of magnitude as for the corresponding polymers. This leads to the conclusion that the elastomers differ mainly from the corresponding polymers in the excess amount of strain due to the crosslinks.

Regarding the wings of the elastomer peaks the situation is somewhat complicated. For MC11-el the tails of the first and second-order peak (Figs. 10b and d) do not permit a reasonable asymptotic fit with a single value of η. This does not allow strong conclusions because probably practical experimental consideration are involved. First the left tail of the second-order peak overlaps somewhat with the right side of the first-order one. Second, due to the relatively large mosaic we could very well be in the transition region between $2 - n^2\eta$ and $1 - n^2\eta$, in which case the asymptotic analysis is unreliable anyhow. In contrast for MeHQ-el we find reasonable scaling with $\eta = 0.17$ from the first harmonic (Fig. 12b) and $\eta = 0.20$ from the second-order peak (Fig. 12d). Finally TR5-el (Fig. 13, right) scales nicely for the higher harmonics with $2 - n^2\eta$ giving $\eta = 0.18 \pm 0.02$ for $n = 3$ and $n = 2$. However, the high-q analysis of the first harmonic (Fig. 13b) leads to a slope < -2 that cannot be interpreted in terms of a value for η. This probably indicates that the dynamic range of the measurement was too small to reach the Caillé limit. Summarizing, the asymptotic behavior as described does not contradict the conclusion of the previous paragraphs.

The observed strain effect on the width of the quasi-Bragg peaks in elastomers can be attributed to layer displacements around topological defects generated in the presence of crosslinks (edge dislocations, dislocation loops). In fact, such dislocations have been observed in smectic side-chain polymers by high-resolution electron microscopy [35]. We expect that defects of higher strength are generated in a large amount upon crosslinking smectic polymers, which causes the large displacement of the layers, $qu \gg 1$. This behavior resembles the predictions for an elastic field of distant dislocations or other topological defects [24]. Similar possibilities have been discussed for various defect situations by Krivoglaz [36]. At high enough strength and density, these defects destroy the algebraic decay of the smectic layer correlations at large distances and lead to a broadening of the Gaussian-like central peak.

Table 2. Results of fitting the FWHM of the elastomers from Table 1 to equation (4).

	Δq_ε $(10^{-3}\,\mathrm{nm}^{-1})$	$\Delta q_{\mathrm{intrinsic}}$ $(10^{-3}\,\mathrm{nm}^{-1})$	Domain size $L_{\mathrm{intrinsic}}$ (nm)
MC11-el	57	42	150
MeHQ-el	85	24	260
TR5-el	60	52	120

According to Table 2 the intrinsic domain size in elastomers can be as small as $L_{\mathrm{intrinsic}} \simeq 200\,\mathrm{nm}$. The question arises whether algebraic decay can survive over such distances. We speculate that in such small-size domains the internal strain due to distant dislocations (or other defects) is strong enough to modify the Caillé correlation function that will be multiplied by another correlation function describing correlations of displacements induced by randomly distributed defects. The resulting power law asymptotes could very well be different from that predicted by the Caillé function only, thus explaining the rather ambiguous results from analysis of the wings of the elastomer peaks. A close look learns that the Lorentzian fits are much less perfect than for the polymers discussed earlier. More seriously, even disregarding some asymmetry, in Figure 10 for MC11-el the deviations are rather different for the first and the second harmonic. The common tendency is that the intensity in the tails of the X-ray peaks is higher than predicted. However, this point is not true for the first harmonic of MeHQ-el (Fig. 12) and the first two harmonics of TR5-el (Fig. 13). In the light of the homopolymer results (attributed to a strong effect of polymer defects on the smectic layer correlations) we assume a complex interplay of these defects and the multiple crosslinks.

Finally we note that in the present main-chain elastomers we did not reach a disordered state as reported for siloxane side-chain elastomers at a concentration of crosslinks of about 20%. Though we investigated chemically very different mesogenic polymers, rather similar cyclic multifunctional crosslinks were involved restricted to a single concentration of about 10%. As the results do not differ much, this could indicate that the influence of the crosslinks on the stability of the smectic elastomer network is stronger than the properties of the smectic matrix. Evidently variation of the crosllink density is needed to make a step towards further understanding.

5 Conclusions

We have investigated the layer correlations in main-chain smectic LC polymer and elastomer systems by X-ray analysis of the lineshape of the corresponding X-ray peak. For the homopolymers these are well described by a Lorentzian, which can be interpreted as an average over domains with dimensions of hundreds of nm. The latter sizes are probably determined by polymer defects (like

hairpins and end points) that are for main-chain LC polymers directly translated into layer distortions. Algebraically decaying order still appears to exist within these domains. The elastomers show much broader peaks than the corresponding polymers. This is attributed to strong non-uniform strain in the finite-size domains that are best described by stretched Gaussians; a Lorentzian description of the lineshapes only holds approximately. This complex behaviour is attributed to the interplay of the polymer defects and the crosslinks leading to strong strains in the finite-size domains.

References

1. P.M. Chaikin, T.C. Lubensky, *Principles of Condensed Matter Physics* (Cambridge University Press, Cambridge, 1995).
2. G. Blatter, M.V. Feigel'man, V.B. Geshkenbein, A.I. Larkin, V.M. Vinokur, Rev. Mod. Phys. **66**, 1125 (1994).
3. R.J. Birgeneau, J. Magn. & Magn. Mater. **177**, 1 (1998).
4. T. Bellini, L. Radzihovsky, J. Toner, N. Clark, Science **294**, 1074 (2001).
5. P.G. de Gennes, J. Prost, *The Physics of Liquid Crystals* (Clarendon, Oxford, 1993).
6. V.P. Shibaev, L. Lam, *Liquid Crystalline and Mesomorphic Polymers* (Springer, New York, Heidelberg, 1999).
7. L.D. Landau, Phys. Z. Sowjetunion **11**, 545 (1937).
8. R.E. Peierls, Helv. Phys. Acta **7**, suppl. II, 81 (1934).
9. M. Warner, E.M. Terentjev, *Liquid Crystal Elastomers* (Clarendon Press, Oxford, 2003).
10. D.M. Lambreva, B.I. Ostrovskii, H. Finkelmann, W.H. de Jeu, Phys. Rev. Lett. **93**, 185702 (2004).
11. E.P. Obraztsov, A.S. Muresan, B.I. Ostrovskii, W.H. de Jeu, to be published in Phys. Rev. E.
12. J. Als-Nielsen, J.D. Litster, R.J. Birgeneau, M. Kaplan, C.R. Safinya, A. Lindegaard-Andersen, S. Mathiesen, Phys. Rev. B **22**, 312 (1980).
13. C.R. Safinya, D. Roux, G.S. Smith, S.K. Sinha, P. Dimon, N.A. Clark, A.M. Bellocq, Phys. Rev. Lett. **57**, 2718 (1986).
14. E. Nachaliel, E.N. Keller, D. Davidov, C. Boeffel, Phys. Rev. A **43**, 2897 (1991).
15. E.M. Terentjev, M. Warner, T.C. Lubensky, Europhys. Lett. **30**, 343 (1995).
16. G.C.L. Wong, W.H. de Jeu, H. Shao, K.S. Liang, R. Zentel, Nature **389**, 576 (1997).
17. P.D. Olmsted, E.M. Terentjev, Phys. Rev. E **53**, 2444 (1996).
18. E.M. Terentjev, Macromol. Symp. **117**, 79 (1997).
19. P. Davidson, A.M. Levelut, Liq. Cryst. **11**, 469 (1992).
20. A.S. Muresan, B.I. Ostrovskii, A. Sanchez-Ferrer, H. Finkelmann, W.H. de Jeu, Eur. Phys. J. E **19**, 385 (2006).
21. A. Sanchez-Ferrer, H. Finkelmann, in preparation.
22. X. Lu, C. He, P. Liu, A.C. Griffin, J. Polym. Sci. A: Polym. Chem. **43**, 3394 (2005).
23. S. Diele, A. Madicke, K. Knauft, J. Neutzler, W. Weissflog, D. Demus, Liq. Cryst. **10**, 47 (1991).
24. V.M. Kaganer, B.I. Ostrovskii, W.H. de Jeu, Phys. Rev. A **44**, 8158 (1991).
25. J.I. Langfort, D. Louer, P. Scardi, J. Appl. Crystallogr. **33**, 964 (2000).
26. P.G. de Gennes, in *Polymer Liquid Crystals*, edited by A. Ciferri, W.R. Krigbaum, R.B. Meyer (Academic, New York, 1982) p. 115.
27. M.H. Li, A. Brulet, J.P. Cotton, P. Davidson, C. Strazielle, P.J. Keller, J. Phys. II **4**, 1843 (1994).
28. A. Vix, W. Stocker, M. Stamm, G. Wilbert, R. Zentel, J.P. Rabe, Macromolecules **31**, 9154 (1998).
29. H. Wermter, H. Finkelmann, e-Polymers **13**, 1 (2001).
30. R.B. Meyer, in *Polymer Liquid Crystals*, edited by A. Ciferri, W.R. Krigbaum, R.B. Meyer (Academic, New York, 1982) p. 133.
31. B.E. Warren, *X-ray Diffraction* (Dover, New York, 1990).
32. G.K. Williamson, W.H. Hall, Acta Metall. **1**, 22 (1953).
33. T. Ungar, A. Borbely, Appl. Phys. Lett. **69**, 3173 (1996).
34. V.M. Kaganer, O. Brandt, A. Trampert, K.H. Ploog, Phys. Rev. B **72**, 045423 (2005).
35. I.G. Voigt-Martin, H. Krug, D. van Dyck, J. Phys. (Paris) **51**, 2347 (1990).
36. M. Krivoglaz, *X-ray and Neutron Diffraction in Non-ideal Crystals* (Springer, Berlin, 1996).